Toxicology Reports 10 (2023) 87–96

Contents lists available at ScienceDirect

Toxicology Reports

journal homepage: www.elsevier.com/locate/toxrep

Detection of β-N-methylamino-L-alanine in postmortem olfactory bulbs of Alzheimer's disease patients using UHPLC-MS/MS: An autopsy case-series study

Susanna P. Garamszegi [a], Sandra Anne Banack [b], Linda L. Duque [a], James S. Metcalf [b], Elijah W. Stommel [c,d], Paul Alan Cox [b], David A. Davis [a,*]

[a] Department of Neurology, University of Miami Miller School of Medicine, Miami, FL 33136, USA
[b] Brain Chemistry Labs, Institute for Ethnomedicine, Jackson, WY 83001, USA
[c] Department of Neurology, Dartmouth-Hitchcock Medical Center Department of Neurology, One Medical Center Dr., Lebanon, NH 03756, USA
[d] Geisel School of Medicine at Dartmouth, Hanover, NH 03755, USA

ARTICLE INFO

Handling Editor: Dr. L.H. Lash

Keywords:
Cyanobacteria
Cyanotoxin
IL-6
Inflammation
Olfactory dysfunction

ABSTRACT

Introduction: Cyanobacterial blooms produce toxins that may become aerosolized, increasing health risks through inhalation exposures. Health related effects on the lower respiratory tract caused by these toxins are becoming better understood. However, nasal exposures to cyanotoxins remain understudied, especially for those with neurotoxic potential. Here, we present a case series study evaluating exposure to β-N-methylamino-L-alanine (BMAA), a cyanobacterial toxin linked to neurodegenerative disease, in postmortem olfactory tissues of individuals with varying stages of Alzheimer's disease (AD).

Methods: Olfactory bulb (*Ob*) tissues were collected during autopsies performed between 2014 and 2017 from six South Florida brain donors (ages 47–78) with residences less than 140 m from a freshwater body. A triple quadrupole tandem mass spectrometry (UHPLC-MS/MS) method validated according to peer AOAC International guidelines was used to detect BMAA and two BMAA isomers: 2,4-diaminobutyric acid (2,4-DAB) and N-(2-aminoethyl)glycine (AEG). Quantitative PCR was performed on the contralateral *Ob* to evaluate the relative expression of genes related to proinflammatory cytokines (*IL-6* & *IL-18*), apoptotic pathways (*CASP1* & *BCL2*), and mitochondrial stress (*IRF1* & *PINK1*). Immunohistochemistry was also performed on the adjacent olfactory tract (*Ot*) to evaluate co-occurring neuropathology with BMAA tissue concentration.

Results: BMAA was detected in the *Ob* of all cases at a median concentration of 30.4 ng/g (Range <LLOQ - 488.4 ng/g). Structural isomers were also detected with median concentrations of 28.8 ng/g (AEG) and 103.6 ng/g (2,4-DAB). In addition, we found that cases with BMAA tissue concentrations above the <LLOQ also displayed increased expression of *IL-6* (3.3-fold), *CASP1* (1.7-fold), and *IRF1* (1.6-fold). Reactive microglial, astrogliosis, myelinopathy, and neuronopathy of axonal processes in the *Ot* were also observed in cases with higher BMAA tissue concentrations.

Conclusion: Our study demonstrates that the cyanobacterial toxin BMAA can be detected in the olfactory pathway, a window to the brain, and its presence may increase the occurrence of proinflammatory cytokines, reactive glia, and toxicity to axonal processes. Further studies will be needed to evaluate BMAA's toxicity via this route of exposure and factors that increase susceptibility.

Abbreviations: AD, Alzheimer's disease; AEG, N-(2-aminoethyl)glycine; ALS/PDC, Amyotrophic lateral sclerosis/ parkinsonism dementia complex; BMAA, β-N-methylamino-L-alanine; CBs, Cyanobacterial blooms; Ob, Olfactory bulb; OD, Olfactory dysfunction; Ot, Olfactory tract; UHPLC-MS/MS, Ultra-performance liquid chromatography and tandem mass spectrometry; 2,4-DAB, 2,4-diaminobutyric acid.

* Corresponding author.
E-mail address: d.davis12@med.miami.edu (D.A. Davis).

https://doi.org/10.1016/j.toxrep.2023.01.002
Received 10 November 2022; Received in revised form 21 December 2022; Accepted 5 January 2023
Available online 6 January 2023

1. Introduction

Olfactory dysfunction (OD) can reduce quality of life, cause depression, and is one of the earliest clinical symptoms of mild cognitive impairment as well as neurodegenerative diseases such as Alzheimer's disease (AD) and Parkinson's disease [1–7]. OD is most commonly contributed to sinonasal disease and upper respiratory tract infections; however, a significant portion of clinical cases are idiopathic in nature [8]. Additionally, there are an increasing number of reports of OD that are linked to acute accidental toxic exposures, as well as chronic exposures to low levels of toxins in the atmosphere [9]. In Florida, cyanobacterial blooms (CBs) occur frequently and produce odorous and taste compounds that interfere with recreational activities and the use of reservoirs for drinking water [10]. CBs produce neurotoxic metabolites that can become aerosolized increasing the risk of inhalation [11,12]. These cyanotoxins have a wide-range of effects, are detectable in the nasal cavity, and exposure doses are dependent on an individual's distance to CBs [13,14]. Once inhaled, these metabolites can cause toxicity at the absorption site, or be mobilized to target organs causing adverse effects [12,15]. The U.S. Center for Disease Control Morbidity and Mortality Weekly Report has shown that harmful CBs are associated with increased emergency room visits for respiratory illnesses [16–19]. More importantly, toxic compounds absorbed into the olfactory epithelium can circumvent the blood brain barrier and gain direct access to the brain [20]. Therefore, exposure to ambient aerosols from CBs should be carefully monitored, especially in susceptible and vulnerable populations [21].

β-N-methylamino-L-alanine (BMAA) is a non-protein amino acid produced by cyanobacteria that has been linked to several neurodegenerative diseases [22–25]. While the toxic effects of BMAA have been primarily reported via ingestion, emerging studies suggest that inhalation exposure may also provide risks for neurological illness [26–28]. This hypothesis is supported by animal models showing that intranasal administration of BMAA can transfer directly to and concentrate in the olfactory bulb (*Ob*) [29]. Direct application of the toxin to olfactory cells causes cell cycle arrest, excitotoxicity, reduced viability with cell death, and decreased mitochondrial function [29–32]. However, studies regarding BMAA exposures involving the human respiratory tract are still emerging [14]. In Florida, recent reports on air sampling of particle associated BMAA has shown that the toxin is detectable in ambient samples collected near active CBs and on home air conditioning filters [11,33]. The reports also noted that BMAA had particle diameters as small as 400 nm and may be ubiquitous to the region [11]. The presence of BMAA particles in ambient air provides a risk for chronic exposure and potential adverse health effects on the olfactory system.

Here, we present an autopsy case-series study evaluating BMAA exposure in the *Ob*, a region responsible for the receipt of neural inputs from the nerves located in the olfactory epithelium of the nasal cavity. BMAA and two BMAA isomers were measured in the *Ob* of Floridians living in close proximity of freshwater bodies with varying stages of AD using a validated method for UHPLC-MS/MS [34,35]. In addition, qPCR and immunohistopathology examinations were performed to determine the relationship between co-occurring BMAA tissue concentrations and markers of inflammation, apoptosis, mitochondrial stress, and olfactory tissue degeneration.

2. Methods

2.1. Case selection and olfactory bulb samples

Six postmortem subjects (47–78 years old) were evaluated for exposure to BMAA toxin and two of its structural isomers: N-(2-aminoethyl)-glycine (AEG) & 2,4-diaminobutyric acid (2,4-DAB), which has also been shown to be neurotoxic in humans (Fig. 1; Table 1) [36]. All biospecimens were collected by and obtained from the University of Miami Brain Endowment Bank biorepository, an NIH NeuroBioBank (Miami, FL, USA). All consents for biospecimen and de-identified data collections were performed in accordance to the University of Miami Institutional Review Board (IRB protocol No. 1992 0348). Subjects were selected based on a sample of convenience from postmortem brain tissues harvested between 2014 and 2017. Clinical, residential, and occupational histories were obtained from medical records, autopsy reports, neuropathology reports, and death certificates. Residential distances to freshwater bodies were determined using Google Earth. AD neuropathological changes of each subject were categorized by a board-certified neuropathologist using the National Institute of Aging Alzheimer Disease Association diagnostic criteria (NIA-AA) (Table 2) [37]. At autopsy, bilateral cranial nerve I samples (n = 6), containing the *Ob* and olfactory tracts (*Ot*) were photographed, dissected, and frozen in 2-methylbutane at −42°C for use in toxicological and gene expression assays. Or, fixed in 10 % neutral buffered formalin for histopathological examination (Fig. 2). The median postmortem interval for this study was 11.5 (3.8 – 26.5) hrs. (Table 2).

2.2. UHPLC-MS/MS

Ob tissue samples were analyzed to verify the presence of BMAA using triple quadrupole tandem mass spectrometry (UHPLC-MS/MS) with a precolumn 6-aminoquinolyl-N-hydroxysuccinimidyl carbamate (AQC) derivatization employing a method validated according to peer AOAC International guidelines and previously reported [34,35,38]. In brief, brain tissue was weighed and hydrolyzed in 6.0 M HCl (200 mg/ml) at 110 °C for 18 hrs. 100 µl of sample was centrifuge/filtered (0.2 µm) at 14,171 x g for 3 min 50 µl of the filtered sample was dried in a Speed-vac under medium heat (1.5 hrs.) and subsequently reconstituted in 500 µl of 20 mM HCl. All samples were derivatized using 20 µl of sample + 60 µl borate buffer mixed with internal standard, D 315 N 2 -BMAA + 20 µl AQC. The final concentration of internal standard in the derivatized sample was 0.055 ng/ml. Each sample was injected three times into the mass spectrometer (3 µl injection volume) and the concentration of each isomer was calculated based on a standard curve with $R^2 = 0.99$ [35]. The limit of detection (LOD) for all three isomers was 0.01 ng/ml and lower limit of quantification (LLOQ) was calculated to be 0.04 ng/ml for each isomer [35]. Analysis was conducted on a Thermo Scientific TSQ Quantiva triple quadrupole mass spectrometer attached to a Thermo Vanquish Ultra High-Pressure Liquid Chromatography Autosampler equipped with a Vanquish pump and heated column compartment. Separation of two BMAA isomers: N-[2-aminoethyl] glycine (AEG), 2,4-diaminobutyric acid (2,4-DAB)) from BMAA was achieved with gradient elution using 20 mM ammonium acetate, pH 5.0 (Fisher Scientific LiChropur™≥ 99 %) (A) and 100

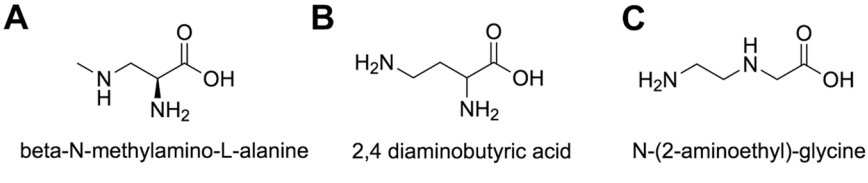

Fig. 1. BMAA and two BMAA isomers. All compounds have a molecular formula of $C_4H_{10}N_2O_2$ and molecular weight of 118.13 g/mol. (**A**) β-N-methylamino-L-alanine or BMAA; IUPAC Name: (2 S)−2-amino-3-(methylamino) propanoic acid; PubChem CID:105089 (**B**) 2,4 diaminobutyric acid or 2,4-DAB; IUPAC Name: 2,4-diaminobutanoic acid; PubChem CID:470. (**C**) N-(2-aminoethyl)-glycine or AEG; IUPAC Name: 2-(2-aminoethylamino)acetic acid; PubChem CID:428913. Compounds were drawn using ChemDraw RRID:SCR_016768.

Table 1
Case demographics

ID	Sex	Age	Race- Ethnicity	Weight (kg)	Height (cm)	BMI	Agonal Health Factors	FL County	Occupation
Case 1	F	47	AA-NH	92.1	160.0	36.0	Obesity	Miami-Dade	Regional manager
Case 2	M	63	C-NH	55.8	177.8	17.7	Interstitial lung disease	St. Lucie	Bridge and tunnel officer
Case 3	F	60	C-H/L	54.4	152.4	23.4	CHF	Broward	Owner-operator: import/export
Case 4	M	75	C-NH	79.4	170.2	27.4	Pleural effusions; CHF	Broward	House keeper/ Painter
Case 5	F	77	C-H/L	50.8	157.5	20.5	Asthma	Miami-Dade	Waitress
Case 6	M	78	C-H/L	70.8	177.8	22.4	Asbestos	Miami-Dade	Auto mechanic
Median:		69		63.3	165.1	22.9			
95 % CI:		47–78		50.8– 92.1	152.4 – 177.8	17.7– 36.0			

AA: African American; **BMI:** body mass index; **C:** Caucasian; **CHF**: congestive heart failure; **cm**: centimeters; **F:** female; **FL:** Florida; **H:** Hispanic; **NH:** non-Hispanic; **kg**: kilograms; **L:** Latino/a/x; **M:** male

Table 2
Postmortem and neuropathological findings

ID	Primary COD	Smoking History	Brain Weight (g)	PMI (hrs.)	Brain pH	RIN	Neuropath Dx	NIA-AA [37] ABC Score
Case 1	Pulmonary embolus	Never	1219	26.5	6.23	6.7	Normal Brain	A0, B0, C0
Case 2	Respiratory failure	Previous	1400	12.9	6.14	7.2	Intermediate AD	A2, B2, C2
Case 3	Congestive heart failure	Previous	700	3.8	5.96	8.7	Advanced AD	A3, B3, C3
Case 4	Cardiopulmonary arrest	Previous	1029	10.1	5.90	8.4	Advanced AD	A3, B3, C3
Case 5	Cardiorespiratory arrest	Previous	1005	7.7	6.21	8.4	Advanced AD	A3, B3, C3
Case 6	Dementia	Previous	1300	20.6	5.49	6.4	Intermediate AD + TDP-43	A3, B2, C3
Median:			1124	11.5	6.05	7.5		
95 % CI:			700 – 1400	3.8 – 26.5	5.49 – 6.23	6.4 – 8.4		

A Score: Thal phase; **B Score:** Braak stage; **C Score:** CERAD; **AD:** Alzheimer's disease; **COD:** cause of death; **Dx:** diagnosis; **hrs.**: hours; **g**: grams; **PMI:** postmortem interval; **RIN:** RNA integrity number

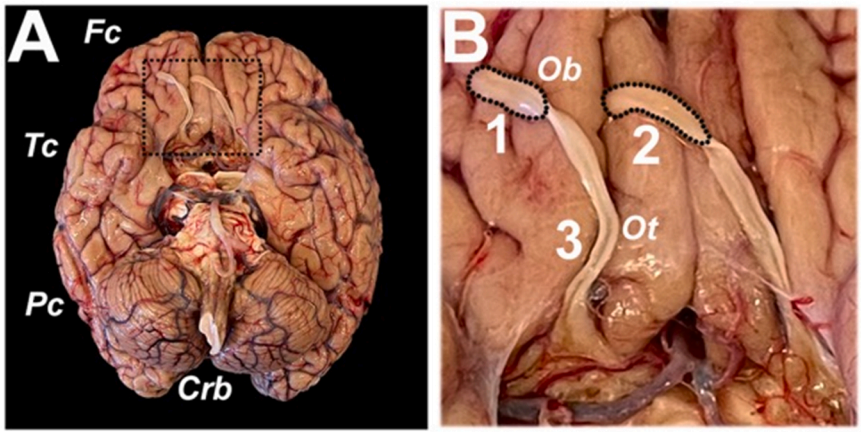

Fig. 2. Olfactory bulb and tract dissection. (**A**) Gross examination of the ventral aspect of the cerebrum, brainstem, and cerebellum from a male with Alzheimer's disease (age 91 years) to highlight the collection and dissection of the olfactory bulb (*Ob*) and tract (*Ot*). *Fc*= frontal cortex; *Tc*= temporal cortex; *Pc*= parietal cortex; *Crb*= cerebellum. (**B**) Higher magnification of the region of interest (black dotted box) shown in panel A. **1:** *Ob* used for UHPLC-MS/MS**; 2:** *Ob* utilized in qPCR experiments and **3:** *Ot* sampled for histopathology analysis. Photograph taken by the University of Miami Brain Endowment Bank.

% methanol (Chromasolv; Honeywell Burdick & Jackson, Muskegon, MI) (B) as follows: flow rate of 0.5 ml/min, initial conditions 10 % B, 1.0 min 10 % B, 4.8 mins 40 % B (curve 5), 5.0 mins 90 % B (curve 5), 6.8 mins 90 % B, 6.81 mins 10 % B (curve 5), and 8 mins 10 % B. Separation was performed using a Thermo Hypersil Gold C-18 column (PN 25002–102130) 100 × 2.1 mm, particle size 1.9 μm heated to 65 °C. Samples were analyzed in positive ion, single reaction monitoring mode using heated electrospray ionization using previously published ion transitions. Mass spectrometer ion source properties were as follows: 3500 V-positive ion, 50 Arb Sheath gas, 10 Arb Aux gas, Sweep gas 0.1 Arb, vaporizer temperature 400 °C, and ion transfer tube temperature 350 °C. Validation curves and parameters were performed as in Glover et al. [34] passing all criteria exceeding minimum requirements for a single-laboratory validation [35]. All samples were run and normalized with an internal BMAA standard (β-N-methyl-D_3-amino-DL-alanine-^{15}N2, Sigma Aldrich Custom Synthesis, 2011). System blanks (AQC derivatized blanks, internal standards, and deionized water) were injected between sample injections.

2.3. RNA extraction, quality control, and cDNA synthesis

Total ribonucleic acid (RNA) was extracted from approximately 100 mg of fresh frozen *Ob* tissue (n = 6) using RNeasy Lipid Tissue Mini Kit with on-column DNase I (Qiagen Inc., Germantown, MD, USA) treatment to eliminate genomic DNA contamination. RNA concentration was measured with NanoDrop 2000 Spectrophotometer (Thermo Scientific, Waltham, MA, USA). Agilent 2100 Bioanalyzer (Agilent Technologies Inc., USA) was used to obtain an RNA integrity number (RIN). The median RIN for our cohort was 7.5 (6.4–8.4) (Table 2). Complementary DNA (cDNA) libraries were generated from 5 μg RNAs in 50 ng/μl concentration using a High Capacity Reverse Transcription Kit (Thermo Fisher Scientific, Waltham, MA, USA).

2.4. Quantitative PCR

Gene expression of proinflammatory cytokines (*IL-6, IL-18*), apoptotic pathways (*BLC2, CASP1*), and mitochondrial stress (*IRF-1, PINK1*) were measured in each sample from 100 ng cDNA per well with TaqMan Universal PCR Master Mix using QuantStudio® 6 Flex Real-Time PCR System (Thermo Fisher Scientific, USA). Human TaqMan assays were purchased from Thermo Fisher Scientific, USA and gene expression levels were normalized to endogenous controls: *GAPDH* and *PPIA*. Gene stability was calculated based on the geNorm algorithm to assist with selecting most stable endogenous controls for data normalization [39,40]. All samples were run in quadruplicate reactions and no template control (NTC) runs were performed for each assay. cDNA was amplified using TaqMan Universal PCR master mix reagent (Thermo Fisher Scientific, USA) at the following conditions: 2 mins at 50 °C, 10 mins at 95 °C, 40 cycles: 15 s at 95 °C and 1 min at 60 °C. The target cDNA for each gene was amplified using TaqMan ABI MGB probe and primer set assays (Table 3). Experimental setup and data analysis were performed using QuantStudio™ Flex Real-Time PCR System Software v1.0 (Thermo Fisher Scientific, USA). All qPCR data files were imported into ExpressionSuite Software v1.0.4 (Applied Biosystems, USA) to analyze relative gene expression across all plates using the comparative Cτ (ΔΔCτ) method [41]. The co-efficient of variation or CV for *GAPDH* Cτ was 0.04 (n = 24 reactions) and *PPIA* Cτ was 0.03 (n = 24 reactions). After normalization of raw data to the geometric mean of the two endogenous controls that met the criteria of no difference between the groups under examinations, relative fold change in gene expression of genes was analyzed ranked in the following exposure groups: AD $^{BMAA\ <LLOQ}$, AD $^{BMAA\ Pos}$, NC $^{BMAA\ Pos}$. Case 3 had the lowest BMAA tissue concentration (<LLOQ) and was used as a normalization control.

2.5. Histopathology and imaging

Formalin-fixed paraffin embedded (FFPE) blocks were prepared from postmortem human *Ot* samples as previously described [50]. *Ot* tissue Section (4 μm) were cut on a microtome (Lecia Biosystems; Deer Park, IL, USA), placed on frosted microscope slides, and stained with hematoxylin and eosin (H&E) at AML laboratories (St. Augustine, FL, USA). For Immunostaining, *Ot* tissue sections were de-paraffinized and treated with Trilogy (Cell Marque Millipore-Sigma; St. Louis, MO, USA) in a water bath at 95 °C for 25 mins. Background Sniper (Biocare Medical; Pacheco, CA, USA) was used for 15 min to reduce nonspecific background staining. *Ot* tissue sections were incubated with anti-glial fibrillary acidic protein (GFAP 1:2000; Abcam Waltham, MA, USA), Ionized calcium binding adaptor molecule 1 (Iba1; 1:1500; FujiFlim Wako Chemicals U.S.A.; Richmond, VA, USA), and anti-tau Alzheimer's disease antibody [GT-38] - Conformation-Specific (1:500, Abcam, Waltham, MA, USA) for 60 mins. Immunostaining was visualized using Mach 2 Rabbit or Mouse HRP polymer (Biocare Medical; Pacheco, CA, USA) for 30 mins, and DAB chromagen (Vector Laboratories; Newark, CA, USA) and CAT hematoxylin counterstain (Biocare Medical; Pacheco, CA, USA). All Immunostaining as well as Luxol Fast Blue (myelin) and periodic acid-Schiff (PAS) staining was performed at The Molecular Pathology Core (University of Florida, Gainesville, FL USA). Digital scans of stained tissue sections were obtained at 40 × (0.2 μm/pixel) magnification using an EasyScan Pro 6 (Motic; Schertz, TX, USA).

Table 3
Target genes and TaqMan qPCR primers

Gene Symbol	Aliases	TaqMan ID #	Function
IL-6	Interleukin 6	Hs00174131_m1	Proinflammatory cytokines, Inflammasome[42–44]
IL-18	Interleukin 18	Hs01038788_m1	
BCL2	BCL2 apoptosis regulator	Hs00236808_s1	Apoptosis, Pyroptosis, Inflammasome[45–47]
CASP1	Caspase 1	Hs00354836_m1	
IRF1	Interferon regulatory factor-1	Hs00971965_m1	Mitochondrial stress[48, 49]
PINK1	PTEN induced kinase 1	Hs00260868_m1	
GAPDH	Glyceraldehyde-3-phosphate dehydrogenase	Hs99999905_m1	Endogenous control[40]
PPIA	Peptidylprolyl isomerase A	Hs99999904_m1	

2.6. Statistical analysis

Statistical analyses were performed using Prism Version 9.5.0 (Graph Pad, San Diego, CA, USA). Multiple comparisons of data sets used a Two-way ANOVA with Dunnett's multiple comparison test. Linear correlations used Spearman's rank correlation coefficient. The Shapiro–Wilk tests were used to determine normality. Data are presented here as the median (95 % CI) or the mean ± standard error with the significance level of alpha = 0.05.

3. Results

3.1. Summary of case demographics

All cases selected for this study lived in residences less than 140 m from a freshwater body and were collected during 3 seasons from 2014 to 2017 (Table 4). The median age was 69 years and one-half (50 %) of the cohort was female (Table 1). Three of six cases (50 %) were Hispanic/Latino/a/x, two of six (33 %) were Caucasian non-Hispanic/Latino/a/x, and one of six (17 %) were African American (Table 1). Five of the six cases (83 %) were retired or not working due to disability from chronic disease. Chronic respiratory exposure risks were primarily due to occupation and were only associated with Case 2 (vehicular exhaust), Case 4 (organic solvents), and Case 6 (asbestos) (Table 1). At time of death, no cases were current smokers and all causes of death were natural (Table 2). Four of six cases (67 %) had agonal health conditions that impeded normal respiratory rates (Table 1). Three of six cases (50 %) had advanced AD, two cases had intermediate AD pathological changes, and one case had a normal adult brain at autopsy (Table 2).

3.2. BMAA and BMAA isomer detection

BMAA and two BMAA Isomers (AEG and 2,4-DAB) were detected in 6 of 6 (100 %) of the *Ob* samples tested (Fig. 3, Table 4). The median concentration of BMAA detected in *Ob* tissues was 30.4 ng/g. Concentrations ranged from below the limit of quantification (<LLOQ) to 488.4 ng/g. AEG was detected in 4 of 6 samples (67 %) with a median concentration of 28.8 ng/g (ND – 56.9 ng/g). In addition, we also detected 2,4-DAB in 6 of 6 donors (100 %) with a median concentration

Table 4
Season of collection, distance to freshwater, and BMAA concentrations detected

ID	YOD	Season	Distance to Freshwater (m)	BMAA (ng/g)	AEG (ng/g)	2,4-DAB (ng/g)
Case 1	2014	Spring	128	30.4	ND	127.7
Case 2	2017	Spring	137	488.4	32.6	81.4
Case 3	2017	Winter	46	<LLOQ	48.2	125.8
Case 4	2016	Fall	70	17.7	56.9	67.8
Case 5	2016	Fall	46	35.4	ND	64.5
Case 6	2016	Winter	21	13.9	24.9	130.3
Median:	2016		58	30.4	28.8	103.6
95 % CI:	2014 – 2017		21 – 137	<LLOQ – 488.4	ND – 56.9	64.5 – 130.3

<LLOQ: below lower limit of quantification; m: meters; ND: not detected; YOD: year of death

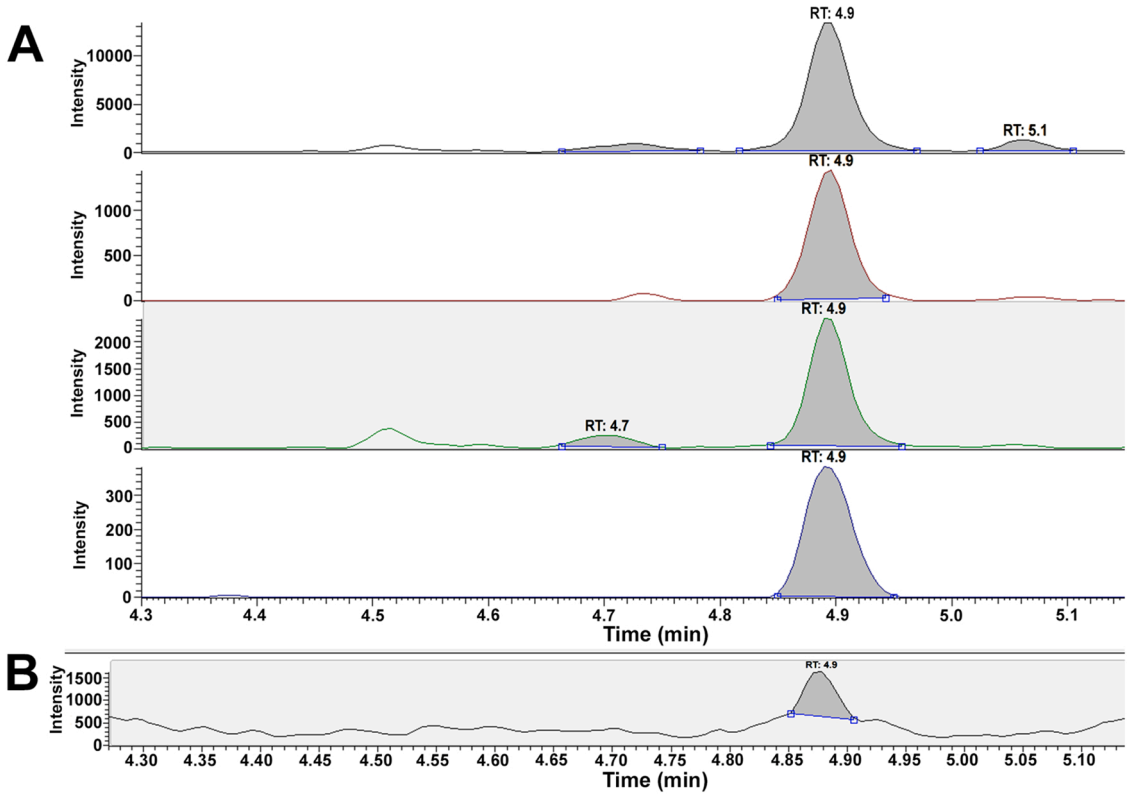

Fig. 3. Detection of BMAA and two BMAA isomers in postmortem olfactory bulb tissue. Triple quadrupole tandem mass spectrometer (UHPLC-MS/MS) analysis of N-(2-aminoethyl)glycine (AEG, 4.7 min), β-N-methylamino-L-alanine (BMAA, 4.9 min), and 2,4-diaminobutyric acid (2,4-DAB, 5.1 min) in the olfactory bulb sampled from postmortem human brain. (**A**) Top four panels represent collision dissociated ions from a parent mass of 459 *m/z* using selective reaction monitoring (from top to bottom: total ion chromatograph, 119 *m/z*, 289 *m/z*, 258 *m/z*). (**B**) Bottom panel represents the total ion chromatograph of the internal stable isotope BMAA standard (0.055 ng/ml) with a parent mass of 464 *m/z*.

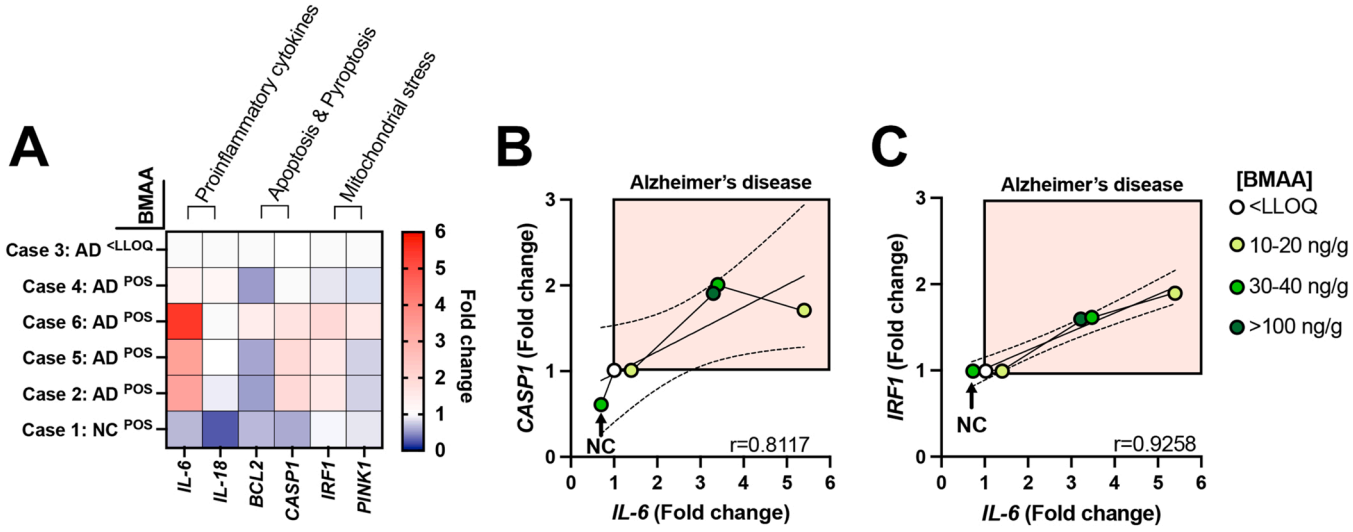

Fig. 4. The BMAA toxin is present in the olfactory bulbs of individuals with elevated expression of genes related to inflammation, cell death, and mitochondrial stress. (A) Heatmaps displaying the fold change of six genes related to proinflammatory cytokines, apoptosis & pyroptosis, inflammasomes, and mitochondrial stress. Gene expression fold change of BMAA ^{POS} and BMAA $^{<LLOQ}$ cases were normalized with endogenous control genes *GAPDH* and *PPIA*. White squares in heatmap indicate baseline gene expression (Fold change = 1). Blue squares indicate genes expressed below the baseline (Fold change < 1). Red squares indicate gene expressed above baseline (Fold change > 1). Interactions accounted for 30.59 % of the total variance (F (25,250) = 18.87; $P < 0.0001$). Whereas, gene expression accounted for 29.81 % of the total variance (F (5, 250) = 91.94; $P < 0.0001$). Finally, case exposure accounted for 22.98 % of the total variance (F (5, 250) = 70.86; $P < 0.0001$). (B, C) *CASP1* (P=0.0361) and *IRF1* (P=0.0167) gene expression was positively correlated with *IL-6* expression in cases with advance Alzheimer's disease (red box). The individual with normal cognition (NC) had the lowest gene expression. The increase in gene expression can be compare to BMAA tissue concentrations for each case: white= <LLOQ (baseline); honeydew= 10–20 ng/g; lime= 30–40 ng/g; moss= >100 ng/g.

of 103.6 ng/g (64.5 – 130.3 ng/g). Tissue concentrations of BMAA, AEG, and 2,4-DAB were neither age nor sex dependent. The highest concentration of BMAA toxin was detected in Case 2 and the lowest in Case 3. The overall trend in these samples was toward a 1:1:3 ratio of BMAA: AEG:DAB. These results represent a small sample size from recent toxin exposure and the significance of this is not known.

3.3. BMAA exposure and olfactory bulb gene expression

Cases with BMAA tissue concentrations that were above the LLOQ displayed upregulated expression of the *IL-6* gene as high as 5.4-fold ($P < 0.0001$, TWO-WAY ANOVA) **(**Fig. 4**,** Table 5**,** Supplemental Table 1**).** The median increase in *IL-6* expression of BMAA ^{POS} vs. BMAA $^{<LLOQ}$ cases was 3.3-fold **(**Table 5**,** Supplemental Table 1**).** Whereas, *IL-18* mRNAs remained relatively unchanged, except for Case 1, a neurologically unaffected control (NC), which had 73 % lower gene expression in comparison to other BMAA ^{POS} AD cases (P=0.0066, TWO-WAY ANOVA) **(**Table 5**,** Supplemental Table 1**).** Proapoptotic *CASP1* expression was also upregulated as high as 2.0-fold in 3 of 5 (60 %) of BMAA ^{POS} cases (P=0.0001, TWO-WAY ANOVA) and was positively correlated with *IL-6* gene expression levels ($r = 0.8117$; P=0.0361, Spearman r) (Fig. 4**B**). Whereas, antiapoptotic *BCL2* expression was decreased in four of five (80 %) of BMAA ^{POS} cases, but results were not statistically significant **(**Table 5**,** Supplemental Table 1**).** *IRF1* gene expression was also significantly upregulated in 2 of 5 (40 %) of BMAA ^{POS} cases (P=0.0002, TWO-WAY ANOVA) and expression was also positively correlated with *IL-6* ($r = 0.9258$; $P = 0.0167$, Spearman r) (Fig. 4**C**). *PINK1* gene expression was relatively unchanged except for Case 6, where expression was upregulated 1.6-fold (P=0.0252, TWO-WAY ANOVA) **(**Table 5**,** Supplemental Table 1**).** Data presented here suggests BMAA exposure may increase expression of genes in the *Ob* related to proinflammatory cytokines, pyroptosis, and mitochondrial stress.

3.4. Olfactory tract histopathology

Varying histopathological changes were observed in the *Ot* of cases evaluated in this study (Fig. 5). We examined available *Ot* samples from cases that died with preclinical (Case 2, Braak III) and advanced AD (Case 3 & Case 5 Braak V-VI). Case 2 and Case 5 display distinct patterns of gliosis and neuropil vacuolation. While, Case 3, an individual with AD and very low BMAA tissue concentration, did not display the same extent of pathological changes (Fig. 5**A-F**). Severe degeneration of axonal processes in the form of neuronopathy (Case 2) and myelinopathy (Case 5) were observed (Fig. 5**H, I**). Whereas, these degenerative changes were not seen in Case 3 (Fig. 5**G**). Various stages of astrogliosis and microglial activation were seen across all cases. However, Case 2 with the highest BMAA exposure displayed severe astrogliosis (Fig. 5**F**) and microglia in a severe hyperactive state (Fig. 5**L**). GT-38 tau positive neurofibrillary tangles were also detected confirming the presences of AD specific neuropathology in cases evaluated (Fig. 5**M-O**)[51].

4. Discussion

BMAA is a non-proteinogenic amino acid produced by cyanobacteria that has been implicated in the high incidence of amyotrophic lateral sclerosis/ parkinsonism dementia complex (ALS/PDC) observed on the island of Guam [22,23,52,53]. The link between BMAA and ALS/PDC is supported by the detection of the toxin in postmortem brains of patients who suffered with the disease and the recapitulation of the neuropathological phenotype in non-human primates and rodents after chronic ingestion [23,38,54–58]. Several modes of toxicity have been proposed for BMAA, which includes actions through glutamate receptors, the cystine/glutamate antiporter (system X_c-), mitochondrial dysfunction, and proteotoxic stress [59–64]. In Florida, the presence of BMAA, its production by cyanobacteria, and its biomagnification in the marine food web has been well documented [10,50,65–70]. In addition, the toxin has been detected in the cerebral cortex and the spinal cord of individuals with AD and ALS, suggesting a potential role as a risk factor for neurodegenerative disease beyond Guam [24,71].

Here we detected and quantified BMAA and two isomers, 2,4-DAB and AEG, in *Ob* brain autopsy specimens obtained from six South Floridians who lived in close proximity to freshwater bodies. All cases regardless of age, sex, disease states, residence, agonal risk factors or season of collection had detectable levels of BMAA in their olfactory tissues. Only one case was below the limit of quantification, but still possessed measurable concentrations of 2,4-DAB and AEG. Tissue concentrations varied across all cases suggesting the levels are most related to individual exposures. In addition, exposures were associated with an increase in the expression of genes related to proinflammatory cytokines, pyroptosis, and mitochondrial stress in our autopsy cohort. The most robust upregulation was seen in *IL-6,* which expression has been shown to be related to hyposmia, inversely correlated with cognitive test scores, and proceeds the development of senile plaques, a hallmark of AD [72–74]. These findings suggest that chronic BMAA exposure to olfactory tissues may increase gene expression profiles that can cause neuroinflammation and olfactory dysfunction in susceptible individuals [75,76].

In AD, olfactory neuropathology consists of degeneration of the olfactory epithelium, atrophy of cranial nerve I, gliosis, inflammation with accompanying senile plaques, neurofibrillary tangles, and in some cases synucleinopathy (Fig. 5) [7,77–81]. In this study, we examined postmortem tissues from the *Ot*, a region containing afferent nerve fibers from mitral and tuft cells located in the *Ob* that connect to the olfactory cortex. BMAA tissue concentrations were associated with more severe degeneration of axonal processes in the olfactory pathway. The degeneration of afferent nerve fibers may be attributed to or exacerbated by the transport of BMAA across the olfactory epithelium in a retrograde fashion like other inhaled toxicants (Fig. 6) [82]. Future studies are

Table 5
BMAA exposure group and olfactory bulb gene expression fold change

ID	Exposure	*IL-6*	*IL-18*	*BCL2*	*CASP1*	*IRF1*	*PINK1*
***Case 3-CTL* vs**	***AD*$^{BMAA\ <LLOQ}$**	*1.0 ± 0.0*	*1.0 ± 0.0*	*1.0 ± 0.0*	*1.0 ± 0.0*	*1.0 ± 0.0*	*1.0 ± 0.0*
Case 6	**AD$^{BMAA\ Pos}$**	5.4 ± 0.2****	1.1 ± 0.0	1.5 ± 0.1	1.7 ± 0.1**	1.9 ± 0.1**	1.6 ± 0.1*
Case 4	**AD$^{BMAA\ Pos}$**	1.4 ± 0.1	1.2 ± 0.1	0.5 ± 0.0	1.0 ± 0.1	1.0 ± 0.1	0.9 ± 0.1
Case 5	**AD$^{BMAA\ Pos}$**	3.4 ± 0.5****	1.0 ± 0.2	0.6 ± 0.0	2.0 ± 0.2***	1.6 ± 0.2*	0.8 ± 0.0
Case 2	**AD$^{BMAA\ Pos}$**	3.3 ± 0.5****	0.9 ± 0.2	0.6 ± 0.0	1.9 ± 0.2***	1.6 ± 0.2	0.8 ± 0.0
Case 1	**NC$^{BMAA\ Pos}$**	0.7 ± 0.0	0.3 ± 0.0**	0.7 ± 0.0	0.6 ± 0.0	1.0 ± 0.0	0.9 ± 0.0
Median$^{(BMAA\ Pos\ Cases)}$:		3.3	1.0	0.6	1.7	1.6	0.9
95 % CI:		0.7 – 5.4	0.3 – 1.2	0.6 – 1.5	0.6 – 2.0	1.0 – 1.9	0.8 – 1.6

AD: Alzheimer's disease; **CTL:** BMAA sample with lowest concentration used for normalization**; NC:** neurologically unaffected control at time of death
* : $P < 0.05$.
** ; $P < 0.01$.
*** ; $P < 0.001$.
**** : $P < 0.0001$ TWO-WAY ANOVA with Dunnett's Multiple Comparison Test.

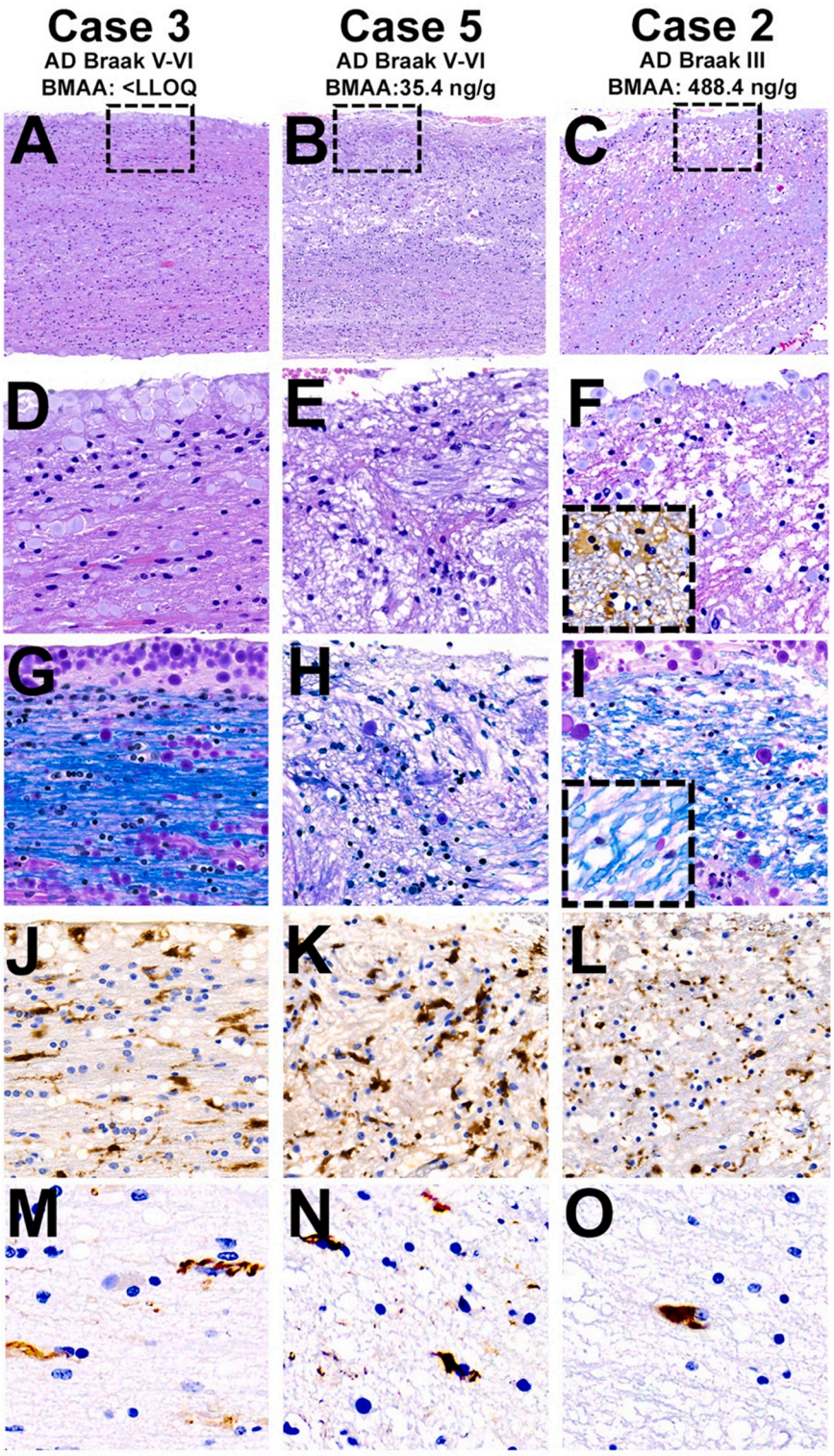

Fig. 5. Co-occurring olfactory tract histopathology in cases with varying BMAA tissue concentrations. (**A-C**) Hematoxylin & eosin (H&E) stained sections of the olfactory tract (*Ot*) from Alzheimer's disease (AD) cases with increasing BMAA tissue concentrations left to right. Case 3 (BMAA: <LLOQ) displays a relatively intact neuropil, whereas, Case 5 (BMAA: 35.4 ng/g) and Case 2 (BMAA: 488.4 ng/g) displays severe neuropil vacuolation. (**D**) Higher magnification of H&E digital scan demonstrates abundant polyglucosan bodies, or *corpora amylacea* (CA), with an organized cellular microenvironment. (**E, F**) Case 5 and Case 2 displaying neuropil vacuolation, gliosis, and a disorganized microenvironment. Black box in panel F highlights astrogliosis with GFAP IHC. (**G**) Luxol fast blue with periodic acid Schiff staining (LFB-PAS) displays numerous CA and myelinated axon fibers. Case 2 and Cases 5 displayed neuronopathy (**H**) and myelinopathy (**I**) Black box in panel I shows high power image of myelin sheath. (**J-L**) Iba1 immunostaining highlights severe reactive microglia in Case 5 and Case 2 relative to Case 3. (**M-O**) GT-38 tau immunostaining highlighting AD specific tau pathology. Digital scan magnification 5x (**A-C**); 20x (**D-L**); 40x (**M-O**).

needed to understand the effect of BMAA on axonal projections in the olfactory tract. As well as studies are needed to determine if the toxin may reach downstream targets in the olfactory cortex, such as the amygdala, which is affected in the earliest stages of AD (Fig. 6) [83].

Lastly, cyanobacteria produce a diverse array of toxic metabolites that can potentially synergize BMAA's toxic effects on the olfactory system [15,84]. Several of these compounds are classified as potent neurotoxins, such as anatoxin-a, cylindrospermopsin, and saxitoxins, and can co-occur with BMAA in aquatic, terrestrial, and atmospheric environments [84–88]. In our autopsy cohort, varying concentrations of BMAA, AEG, and 2,4-DAB were detected in olfactory tissues. The combination of all three BMAA compounds, could result in synergistic cytotoxicity [89–91]. Likewise, other co-occurring cyanobacterial toxins such as microcystin-LR, components of cyanobacteria such as lipopolysaccharide or LPS, and heavy metals like mercury that can concentrate in the *Ob* should also be considered due to their synergy with BMAA [20, 92–95]. Future studies are needed to understand how co-exposures to multiple cyanotoxins and other compounds in the environment impact

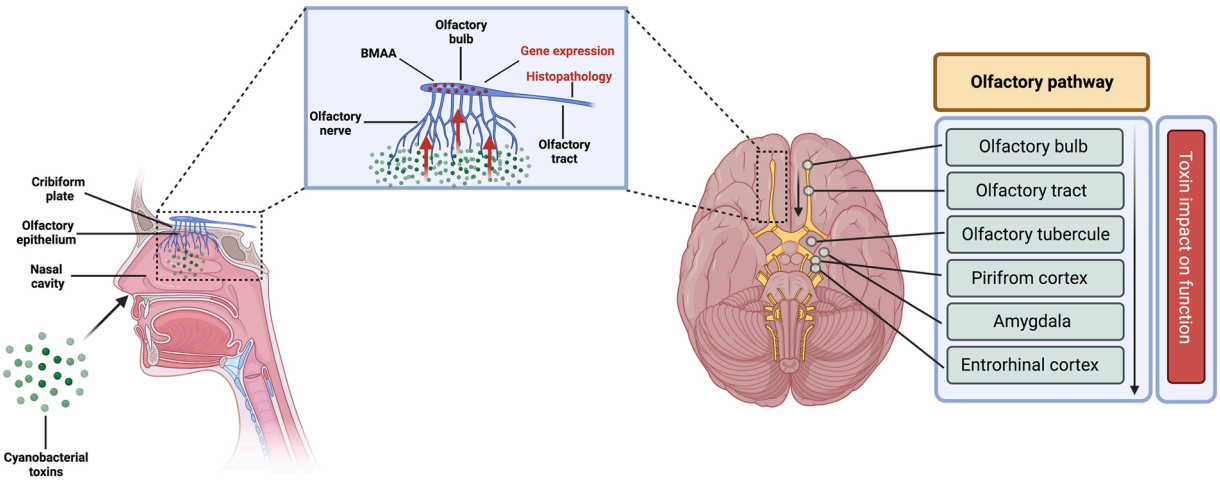

Fig. 6. BMAA inhalation exposure and potential targets of the olfactory pathway. BMAA particles from cyanobacteria that are aerosolized may be inhaled into the nasal cavity where they can cross the olfactory epithelium to deposit into the olfactory bulb (*Ob*). In the *Ob,* BMAA may upregulate the expression of genes related to proinflammatory cytokines, mitochondrial stress, and cell death. BMAA, like other inhaled toxins, may transport in a retrograde manner along the olfactory pathway where it could deposit deep into transentorhinal regions. The presence of the BMAA toxin in these regions may exacerbate clinical symptoms of Alzheimer's disease. Designed with BioRender.

the olfactory pathway and brain health.

5. Conclusion

In our case series study, the cyanobacterial toxin BMAA and two of its isomers AEG and 2,4-DAB, were detected in olfactory tissues taken from postmortem brains with varying stages of AD. In addition, elevated expression of *IL-6*, *CASP1*, and *IRF1* genes were observed in the *Ob* of AD brains, where BMAA concentrations were well above the lower limit of quantification. Finally, the presence of the BMAA toxin in the olfactory microenvironment may exacerbate ongoing neuronal and glial toxicity.

Funding

This research was funded by the Herbert W. Hoover Foundation, The William Stamps Farish Fund, and the Josephine P. & John J. Louis Foundation.

CRediT authorship contribution statement

SPG: perform experiments, analyzed data, edited the manuscript, **SAB:** perform experiments, analyzed data, edited the manuscript, **LLD:** analyzed data, **JSM:** edited the manuscript, **EWS:** edited the manuscript, **PAC:** edited the manuscript, **DAD:** conceived the project, perform experiments, analyzed data, and wrote the manuscript.

Declaration of Competing Interest

The authors declare that they have no known competing financial interests or personal relationships that could have appeared to influence the work reported in this paper.

Data availability

Data will be made available on request.

Acknowledgments

We thank Josephine W. Ashmead, Thomas M. Coyne, and Kenneth D. Hutchins for providing neuropathological review of our case cohort. We also like to thank Walter G. Bradley and Larry E. Brand for their discussions and review of this manuscript. We are grateful for the assistance of Nathalie Augustine-Adras, Wizner J. Canate, and Willie J. Chance, II for performing postmortem tissue recoveries and gross tissue imaging. We wish to acknowledge Angela M. Amatruda, HT (ASCP) and the staff at AML Laboratories, Saint Augustine, FL for providing the application of H&E stains. We also acknowledge Dongtao Ann Fu and Yuping Cathy Sun at the Molecular Pathology Core at the University of Florida, Gainesville, FL for providing immunohistochemistry services. We also like to recognize the staff at the University of Miami Brain Endowment Bank, an NIH NeuroBioBank, for providing the donated postmortem Alzheimer's disease brain tissues used in these studies.

Appendix A. Supporting information

Supplementary data associated with this article can be found in the online version at doi:10.1016/j.toxrep.2023.01.002.

References

[1] I. Croy, S. Nordin, T. Hummel, Olfactory disorders and quality of life–an updated review, Chem. Senses 39 (3) (2014) 185–194.
[2] Y. Mai, et al., Well-being in patients with olfactory dysfunction, Physiol. Behav. 254 (2022), 113899.
[3] R.L. Doty, Olfactory dysfunction in Parkinson disease, Nat. Rev. Neurol. 8 (6) (2012) 329–339.
[4] M. Pardini, et al., Olfactory function in corticobasal syndrome and frontotemporal dementia, Arch. Neurol. 66 (1) (2009) 92–96.
[5] R.L. Doty, Olfactory dysfunction in neurodegenerative diseases: is there a common pathological substrate? Lancet Neurol. 16 (6) (2017) 478–488.
[6] P. Kohli, et al., The association between olfaction and depression: a systematic review, Chem. Senses 41 (6) (2016) 479–486.
[7] R.O. Roberts, et al., Association between olfactory dysfunction and amnestic mild cognitive impairment and Alzheimer disease dementia, JAMA Neurol. 73 (1) (2016) 93–101.
[8] A.F. Temmel, et al., Characteristics of olfactory disorders in relation to major causes of olfactory loss, Arch. Otolaryngol. Head. Neck Surg. 128 (6) (2002) 635–641.
[9] U.D. Upadhyay, E.H. Holbrook, Olfactory loss as a result of toxic exposure, Otolaryngol. Clin. North Am. 37 (6) (2004) 1185–1207.
[10] J. Burns, Toxic cyanobacteria in Florida waters, Adv. Exp. Med Biol. 619 (2008) 127–137.
[11] M.L. Parsons, J. Peccia, W. Arnold, Preliminary Report on Air Sampling of Particle-Associated Microcystins and BMAA Pilot Study in Lee County, Florida: Fall 2018 – Winter 2019, Florida Gulf Coast University, 2019.
[12] J.S. Metcalf, et al., Cyanotoxins and the nervous system, Toxins (Basel) 13 (9) (2021).
[13] A.M. Schaefer, et al., Exposure to microcystin among coastal residents during a cyanobacteria bloom in Florida, Harmful Algae 92 (2020), 101769.
[14] D.N. Facciponte, et al., Identifying aerosolized cyanobacteria in the human respiratory tract: a proposed mechanism for cyanotoxin-associated diseases, Sci. Total Environ. 645 (2018) 1003–1013.

[15] H.E. Plaas, H.W. Paerl, Toxic cyanobacteria: a growing threat to water and air quality, Environ. Sci. Technol. 55 (1) (2021) 44–64.
[16] J. Wu, et al., Acute health effects associated with satellite-determined cyanobacterial blooms in a drinking water source in Massachusetts, Environ. Health 20 (1) (2021) 83.
[17] A.M. Lavery, et al., Evaluation of syndromic surveillance data for studying harmful algal bloom-associated illnesses - United States, 2017-2019, MMWR Morb. Mortal. Wkly Rep. 70 (35) (2021) 1191–1194.
[18] V.A. Roberts, et al., Surveillance for harmful algal bloom events and associated human and animal illnesses - one health harmful algal bloom system, United States, 2016-2018, MMWR Morb. Mortal. Wkly Rep. 69 (50) (2020) 1889–1894.
[19] M. Figgatt, et al., Harmful algal bloom-associated illnesses in humans and dogs identified through a pilot surveillance system - New York, 2015, MMWR Morb. Mortal. Wkly Rep. 66 (43) (2017) 1182–1184.
[20] F.W. Sunderman Jr., Nasal toxicity, carcinogenicity, and olfactory uptake of metals, Ann. Clin. Lab Sci. 31 (1) (2001) 3–24.
[21] L.G. Hooper, J.D. Kaufman, Ambient air pollution and clinical implications for susceptible populations, Ann. Am. Thorac. Soc. 15 (Suppl 2) (2018) S64–S68.
[22] P.A. Cox, O.W. Sacks, Cycad neurotoxins, consumption of flying foxes, and ALS-PDC disease in Guam, Neurology 58 (6) (2002) 956–959.
[23] P.S. Spencer, et al., Guam amyotrophic lateral sclerosis-parkinsonism-dementia linked to a plant excitant neurotoxin, Science 237 (4814) (1987) 517–522.
[24] J. Pablo, et al., Cyanobacterial neurotoxin BMAA in ALS and Alzheimer's disease, Acta Neurol. Scand. 120 (4) (2009) 216–225.
[25] M.E. Newell, S. Adhikari, R.U. Halden, Systematic and state-of the science review of the role of environmental factors in Amyotrophic Lateral Sclerosis (ALS) or Lou Gehrig's Disease, Sci. Total Environ. 817 (2022), 152504.
[26] P.A. Cox, et al., Cyanobacteria and BMAA exposure from desert dust: a possible link to sporadic ALS among Gulf War veterans, Amyotroph. Lateral Scler. 10 Suppl 2 (2009) 109–117.
[27] J.S. Metcalf, et al., Cyanotoxins in desert environments may present a risk to human health, Sci. Total Environ. 421–422 (2012) 118–123.
[28] S.A. Banack, et al., Detection of cyanotoxins, beta-N-methylamino-L-alanine and microcystins, from a lake surrounded by cases of amyotrophic lateral sclerosis, Toxins (Basel) 7 (2) (2015) 322–336.
[29] P. Pierozan, et al., The cyanobacterial neurotoxin beta-N-methylamino-L-alanine (BMAA) targets the olfactory bulb region, Arch. Toxicol. 94 (8) (2020) 2799–2808.
[30] A.S. Chiu, et al., Gliotoxicity of the cyanotoxin, beta-methyl-amino-L-alanine (BMAA), Sci. Rep. 3 (2013) 1482.
[31] A.S. Chiu, et al., Global cellular responses to beta-methyl-amino-L-alanine (BMAA) by olfactory ensheathing glial cells (OEC), Toxicon 99 (2015) 136–145.
[32] J. Hu, et al., Exposure to aerosolized algal toxins in south florida increases short- and long-term health risk in drosophila model of aging, Toxins (Basel) 12 (12) (2020).
[33] C. Waterkeeper, Collaborative Research on Airborne Toxins from Harmful Algal Blooms in Southwest Florida. News Post, Calusa Waterkeeper Ft., Myers, FL, 2022.
[34] W.B. Glover, et al., Determination of beta-N-methylamino-L-alanine, N-(2-aminoethyl)glycine, and 2,4-diaminobutyric acid in food products containing cyanobacteria by ultra-performance liquid chromatography and tandem mass spectrometry: single-laboratory validation, J. AOAC Int 98 (6) (2015) 1559–1565.
[35] S.A. Banack, Second laboratory validation of beta-N-methylamino-L-alanine, N-(2aminoethyl)glycine, and 2,4-diaminobuytric acid by ultra-performance liquid chromatography and tandem mass spectrometry, Neurotox. Res 39 (1) (2021) 107–116.
[36] T. Schneider, et al., Neurotoxicity of isomers of the environmental toxin L-BMAA, Toxicon 184 (2020) 175–179.
[37] T.J. Montine, et al., National Institute on Aging-Alzheimer's Association guidelines for the neuropathologic assessment of Alzheimer's disease: a practical approach, Acta Neuropathol. 123 (1) (2012) 1–11.
[38] S.A. Banack, P.A. Cox, Creating a simian model of guam ALS/PDC which reflects chamorro lifetime BMAA exposures, Neurotox. Res 33 (1) (2018) 24–32.
[39] J. Vandesompele, et al., Accurate normalization of real-time quantitative RT-PCR data by geometric averaging of multiple internal control genes, Genome Biol. 3 (7) (2002). RESEARCH0034.
[40] Q. Zhang, et al., Comparison of reference genes for transcriptional studies in postmortem human brain tissue under different conditions, Neurosci. Bull. 35 (2) (2019) 225–228.
[41] T.D. Schmittgen, K.J. Livak, Analyzing real-time PCR data by the comparative C(T) method, Nat. Protoc. 3 (6) (2008) 1101–1108.
[42] T. Tanaka, M. Narazaki, T. Kishimoto, IL-6 in inflammation, immunity, and disease, Cold Spring Harb. Perspect. Biol. 6 (10) (2014) a016295.
[43] C.A. Dinarello, et al., Interleukin-18 and IL-18 binding protein, Front Immunol. 4 (2013) 289.
[44] F.L. van de Veerdonk, et al., Inflammasome activation and IL-1beta and IL-18 processing during infection, Trends Immunol. 32 (3) (2011) 110–116.
[45] J. Kale, E.J. Osterlund, D.W. Andrews, BCL-2 family proteins: changing partners in the dance towards death, Cell Death Differ. 25 (1) (2018) 65–80.
[46] S. Shalini, et al., Old, new and emerging functions of caspases, Cell Death Differ. 22 (4) (2015) 526–539.
[47] T. Bergsbaken, S.L. Fink, B.T. Cookson, Pyroptosis: host cell death and inflammation, Nat. Rev. Microbiol 7 (2) (2009) 99–109.
[48] S.Y. Deng, et al., Role of interferon regulatory factor-1 in lipopolysaccharide-induced mitochondrial damage and oxidative stress responses in macrophages, Int J. Mol. Med 40 (4) (2017) 1261–1269.
[49] C.A. Gautier, T. Kitada, J. Shen, Loss of PINK1 causes mitochondrial functional defects and increased sensitivity to oxidative stress, Proc. Natl. Acad. Sci. USA 105 (32) (2008) 11364–11369.
[50] D.A. Davis, et al., Cyanobacterial neurotoxin BMAA and brain pathology in stranded dolphins, PLoS One 14 (3) (2019), e0213346.
[51] G.S. Gibbons, et al., Detection of Alzheimer disease (AD)-specific tau pathology in AD and NonAD tauopathies by immunohistochemistry with novel conformation-selective tau antibodies, J. Neuropathol. Exp. Neurol. 77 (3) (2018) 216–228.
[52] P.A. Cox, R.M. Kostrzewa, G.J. Guillemin, BMAA and neurodegenerative illness, Neurotox. Res 33 (1) (2018) 178–183.
[53] S.A. Banack, S.J. Murch, P.A. Cox, Neurotoxic flying foxes as dietary items for the Chamorro people, Marianas Islands, J. Ethnopharmacol. 106 (1) (2006) 97–104.
[54] P.A. Cox, et al., Dietary exposure to an environmental toxin triggers neurofibrillary tangles and amyloid deposits in the brain, Proc. Biol. Sci. 283 (1823) (2016).
[55] D.A. Davis, et al., l-Serine reduces spinal cord pathology in a vervet model of preclinical ALS/MND, J. Neuropathol. Exp. Neurol. 79 (4) (2020) 393–406.
[56] S.J. Murch, et al., Occurrence of beta-methylamino-l-alanine (BMAA) in ALS/PDC patients from Guam, Acta Neurol. Scand. 110 (4) (2004) 267–269.
[57] H.Z. Yin, et al., Intrathecal infusion of BMAA induces selective motor neuron damage and astrogliosis in the ventral horn of the spinal cord, Exp. Neurol. 261 (2014) 1–9.
[58] L.L. Scott, T.G. Downing, A single neonatal exposure to BMAA in a rat model produces neuropathology consistent with neurodegenerative diseases, Toxins (Basel) 10 (1) (2017).
[59] A.S. Chiu, et al., Excitotoxic potential of the cyanotoxin beta-methyl-amino-L-alanine (BMAA) in primary human neurons, Toxicon 60 (6) (2012) 1159–1165.
[60] R.A. Dunlop, et al., The non-protein amino acid BMAA is misincorporated into human proteins in place of L-serine causing protein misfolding and aggregation, PLoS One 8 (9) (2013), e75376.
[61] B.J. Main, R.A. Dunlop, K.J. Rodgers, The use of L-serine to prevent beta-methylamino-L-alanine (BMAA)-induced proteotoxic stress in vitro, Toxicon 109 (2016) 7–12.
[62] R. Albano, D. Lobner, Transport of BMAA into neurons and astrocytes by system xc, Neurotox. Res 33 (1) (2018) 1–5.
[63] D. Lobner, et al., Beta-N-methylamino-L-alanine enhances neurotoxicity through multiple mechanisms, Neurobiol. Dis. 25 (2) (2007) 360–366.
[64] D.F. Silva, et al., Microbial BMAA elicits mitochondrial dysfunction, innate immunity activation, and Alzheimer's disease features in cortical neurons, J. Neuroinflamm. 17 (1) (2020) 332.
[65] L.E. Brand, Human exposure to cyanobacteria and BMAA, Amyotroph. Lateral Scler. 10 Suppl 2 (2009) 85–95.
[66] L.E. Brand, et al., Cyanobacterial blooms and the occurrence of the neurotoxin beta-N-methylamino-L-alanine (BMAA) in South Florida aquatic food webs, Harmful Algae 9 (6) (2010) 620–635.
[67] N. Hammerschlag, et al., Cyanobacterial neurotoxin BMAA and mercury in sharks, Toxins (Basel) 8 (8) (2016).
[68] K. Mondo, et al., Cyanobacterial neurotoxin beta-N-methylamino-L-alanine (BMAA) in shark fins, Mar. Drugs 10 (2) (2012) 509–520.
[69] J.S. Metcalf, et al., Toxin analysis of freshwater cyanobacterial and marine harmful algal blooms on the west coast of florida and implications for estuarine environments, Neurotox. Res 39 (1) (2021) 27–35.
[70] S.A. Banack, et al., Detection of cyanobacterial neurotoxin beta-N-methylamino-l-alanine within shellfish in the diet of an ALS patient in Florida, Toxicon 90 (2014) 167–173.
[71] W.G. Bradley, D.C. Mash, Beyond Guam: the cyanobacteria/BMAA hypothesis of the cause of ALS and other neurodegenerative diseases, Amyotroph. Lateral Scler. 10 Suppl 2 (2009) 7–20.
[72] M. Hull, et al., Interleukin-6-associated inflammatory processes in Alzheimer's disease: new therapeutic options, Neurobiol. Aging 17 (5) (1996) 795–800.
[73] K.S.P. Lai, et al., Peripheral inflammatory markers in Alzheimer's disease: a systematic review and meta-analysis of 175 studies, J. Neurol. Neurosurg. Psychiatry 88 (10) (2017) 876–882.
[74] R.I. Henkin, L. Schmidt, I. Velicu, Interleukin 6 in hyposmia, JAMA Otolaryngol. Head. Neck Surg. 139 (7) (2013) 728–734.
[75] M. Erta, A. Quintana, J. Hidalgo, Interleukin-6, a major cytokine in the central nervous system, Int J. Biol. Sci. 8 (9) (2012) 1254–1266.
[76] S. Méressea, et al., β-N-Methyl-Amino-L-Alanine cyanotoxin promotes modification of undifferentiated cells population and disrupts the inflammatory status in primary cultures of neural stem cells, Toxicology 482 (2022).
[77] R.L. Doty, V. Kamath, The influences of age on olfaction: a review, Front Psychol. 5 (2014) 20.
[78] J. Attems, L. Walker, K.A. Jellinger, Olfaction and aging: a mini-review, Gerontology 61 (6) (2015) 485–490.
[79] C. Murphy, Olfactory and other sensory impairments in Alzheimer disease, Nat. Rev. Neurol. 15 (1) (2019) 11–24.
[80] T.G. Beach, et al., Olfactory bulb alpha-synucleinopathy has high specificity and sensitivity for Lewy body disorders, Acta Neuropathol. 117 (2) (2009) 169–174.
[81] S.E. Arnold, et al., Olfactory epithelium amyloid-beta and paired helical filament-tau pathology in Alzheimer disease, Ann. Neurol. 67 (4) (2010) 462–469.
[82] H. Tjalve, J. Henriksson, Uptake of metals in the brain via olfactory pathways, Neurotoxicology 20 (2–3) (1999) 181–195.
[83] H. Braak, E. Braak, Neuropathological stageing of Alzheimer-related changes, Acta Neuropathol. 82 (4) (1991) 239–259.
[84] J. Huisman, et al., Cyanobacterial blooms, Nat. Rev. Microbiol 16 (8) (2018) 471–483.

[85] J.W. Sutherland, et al., The detection of airborne anatoxin-a (ATX) on glass fiber filters during a harmful algal bloom, Lake Reserv. Manag. 37 (2) (2021) 13–119.
[86] G. Grtner, M. Stoyneva-Grtner, B. Uzunov, Algal toxic compounds and their aeroterrestrial, airborne and other extremophilic producers with attention to soil and plant contamination: a review, Toxins (Basel) 13 (5) (2021).
[87] M.A. Al-Sammak, et al., Co-occurrence of the cyanotoxins BMAA, DABA and anatoxin-a in Nebraska reservoirs, fish, and aquatic plants, Toxins (Basel) 6 (2) (2014) 488–508.
[88] J.S. Metcalf, G.A. Codd, Co-occurrence of cyanobacteria and cyanotoxins with other environmental health hazards: impacts and implications, Toxins (Basel) 12 (10) (2020).
[89] R.M. Martin, J. Stallrich, M.S. Bereman, Mixture designs to investigate adverse effects upon co-exposure to environmental cyanotoxins, Toxicology 421 (2019) 74–83.
[90] B.J. Main, K.J. Rodgers, Assessing the combined toxicity of BMAA and its isomers 2,4-DAB and AEG in vitro using human neuroblastoma cells, Neurotox. Res 33 (1) (2018) 33–42.
[91] V.X. Tan, et al., Detection of the cyanotoxins L-BMAA uptake and accumulation in primary neurons and astrocytes, Neurotox. Res 33 (1) (2018) 55–61.
[92] R.M. Martin, M.S. Bereman, K.C. Marsden, BMAA and MCLR interact to modulate behavior and exacerbate molecular changes related to neurodegeneration in larval zebrafish, Toxicol. Sci. 179 (2) (2021) 251–261.
[93] D.A. Davis, et al., BMAA, methylmercury, and mechanisms of neurodegeneration in dolphins: a natural model of toxin exposure, Toxins (Basel) 13 (10) (2021).
[94] T. Rush, X. Liu, D. Lobner, Synergistic toxicity of the environmental neurotoxins methylmercury and beta-N-methylamino-L-alanine, Neuroreport 23 (4) (2012) 216–219.
[95] Q. He, et al., Intranasal LPS-mediated Parkinson's model challenges the pathogenesis of nasal cavity and environmental toxins, PLoS One 8 (11) (2013), e78418.